with negative χ_1 torsion angle adopts the B form, and the other three rings with positive χ_1 values adopt the A form (Table V). In the $(GPPGPP)_2Mg$ crystal, however, instead of one, there are two pyrrolidine rings of each independent molecule that adopt the B form.

The pyramidality of the N atoms of the proline moieties of the molecule is negligible as their deviations from the planes formed by their immediate three neighbor atoms are less than 0.08 Å. Moreover the difference of the two torsion angles ($\theta''_i - \phi_i$), which gives a measure of the coplanarity of the bonds connected to the N atom, approximates 180° for each proline unit with a maximum deviation of 9.8° (Table V).

C–C bond lengths in the pyrrolidine rings vary between 1.515 and 1.536 Å with the exception of $C^{\beta}{}_6 - C^{\gamma}{}_6$ and $C^{\gamma}{}_6 - C^{\delta}{}_6$, which have been found to be as short as 1.413 and 1.456 Å, respectively (Table IV). These extraordinarily short bond lengths may be partly attributed to the high thermal vibration or unresolved positional disorder of $C^{\beta}{}_6$ and $C^{\gamma}{}_6$. It is noteworthy to mention that for the same pyrrolidine ring in both independent molecules of the $(GPPGPP)_2Mg$ complex these two bonds show similar deviations with values of 1.449 and 1.499 Å, respectively. The N–C^{α} bond lengths in the two glycine units 1.445 and 1.447 Å are shorter than those in the pyrrolidine rings, for which the average N–C^{α} bond length is 1.471 Å with a maximum deviation of 0.006 Å. This difference of N–C^{α} bonds in glycine and proline units is not so firmly expressed in the crystal structure of $(GPPGPP)_2Mg$ complex whereas the individual values show some deviations.

Similar to the bond lengths, the corresponding bond angles of the different peptide units also show smaller deviations in the uncomplexed hexapeptide than in the complexed one, but when the average values of the same angles are taken, they are nearly the same in both structures.

Acknowledgment. We are grateful for the crystals supplied by Professor L. Radics.

Registry No. $GPPGPP \cdot 3H_2O$, 81847-24-7.

Supplementary Material Available: Listing of observed and calculated structure factors as well as tables of anisotropic thermal parameters of non-hydrogen atoms, coordinates of hydrogen atoms, best planes of the pyrrolidine rings and glycine moieties of the molecule together with their dihedral angles, pyramidality of the N atoms of the proline moieties, and intermolecular contact distances other than hydrogen bonds (26 pages). Ordering information is given on any current masthead page.

(14) Ashida, T.; Kakudo, M. *Bull. Chem. Soc. Jpn.* **1974**, *47*, 1129–1133.

Kinetic Studies on the Formation of Two Intramolecular Excimers in Substituted Dinaphthylpropanes

Hideyuki Itagaki,* Noriko Obukata, Akio Okamoto, Kazuyuki Horie, and Itaru Mita

Contribution from the Institute of Interdisciplinary Research, Komaba Campus, Faculty of Engineering, University of Tokyo, Komaba, Meguro-ku, Tokyo 153, Japan.
Received October 5, 1981

Abstract: The emission properties of 1,3-bis(4-methoxy-1-naphthyl)propane (BMNP) and 1,3-bis(4-hydroxy-1-naphthyl)propane (BHNP) have been investigated in fluid solution. They exhibit, in addition to the monomer fluorescence, two structureless emissions derived from two different types of excimer: a normal excimer and a second excimer, the latter having a partially overlapping structure of aromatic rings. The kinetic analysis of transient decay curves for the fluorescence of BMNP showed that the second excimer is not formed from or converted to the normal excimer and that the two are formed independently from the excited monomer. Some activation energies and rate constants were determined. The activation energy for the second excimer formation was found to be smaller than that of the normal excimer formation.

Numerous investigations of a so-called second excimer in poly(*N*-vinylcarbazole) (PVCz) and its derivatives in fluid solution have been reported.[1-7] While the stable "normal excimer" configuration is reported to be a symmetrical sandwich arrangement,[8] the second excimer may have a partially overlapped sandwich structure of two aromatic rings.[3,4] The emission characteristics of such excimers must be sensitive to the structure and conformation of polymers, and actually there exists a significant difference in emission between isotactic-rich PVCz derivatives and ones rich in syndiotactic structure.[3,4,6,7] However, the elucidation of the second excimer formation and its application to investigate the conformation of polymers should be clearly distinguished, because of the possible occurrence of energy migration and other complicating phenomena in polymers.

A useful approach for studying the intramolecular excimer formation in vinyl polymers, which is inherently complex due to a large number of possible configurations, is to consider first simpler model systems in which two chromophores are attached to 1,3-positions of a propane chain. Investigations of such dimer models corresponding to the "$n = 3$ rule", first studied by Hirayama for diphenyl- and triphenylalkanes,[9] have been carried out for dinaphthylalkanes by Chandross and Dempster,[8] for 1,3-bis(*N*-carbazoyl)propane by Klöpffer[10] and Johnson,[11] and for dipyrenylalkanes by Zachariasse.[12] However, the dimer models

(1) David, C.; Piens, M.; Gueskens, G. *Eur. Polym. J.* **1972**, *8*, 1291.
(2) Johnson, G. E. *J. Chem. Phys.* **1975**, *62*, 4697.
(3) Itaya, A.; Okamoto, K.; Kusabayashi, S. *Bull. Chem. Soc. Jpn.* **1976**, *49*, 2082.
(4) Itaya, A.; Okamoto, K.; Kusabayashi, S. *Bull. Chem. Soc. Jpn.* **1978**, *51*, 79.
(5) Hoyle, C. E.; Nemzek, T. L.; Mar, A.; Guillet, J. E. *Macromolecules* **1978**, *11*, 429.
(6) Houben, J. L.; Natucci, B.; Solaro, R.; Colella, O.; Chiellini, E.; Ledwith, A. *Polymer* **1978**, *19*, 811.
(7) Johnson, G. E.; Keyanpour-Rad, M.; Ledwith, A. *Macromolecules* **1980**, *13*, 222.
(8) Chandross, E. A.; Dempster, C. J. *J. Am. Chem. Soc.* **1970**, *92*, 3586.
(9) Hirayama, F. *J. Chem. Phys.* **1965**, *42*, 3163.
(10) Klöpffer, W. *Chem. Phys. Lett.* **1969**, *4*, 193.
(11) Johnson, G. E. *J. Chem. Phys.* **1974**, *61*, 3002.
(12) Zachariasse, K.; Küknle, W. *Z. Phys. Chem. (Wiesbaden)* **1976**, *101*, 267.

0002-7863/82/1504-4469$01.25/0

Scheme I

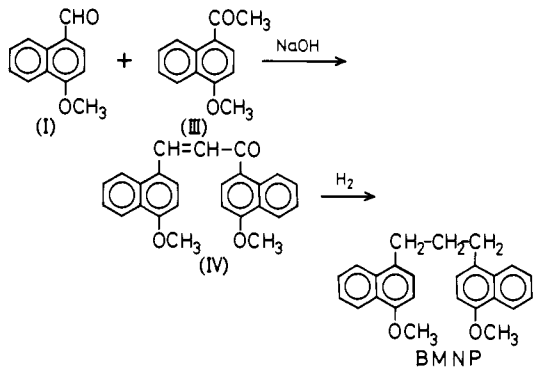

for PVCz did not show the second excimer emission,[10,11] and this makes more difficult the elucidation of phenomena of the second excimer in this polymer.

Except PVCz, few compounds are known to give more than one excimer having a different overlapping structure of aromatic rings; they are dianthrylethanes, studied by Mataga,[13] and dianthrylpropane, studied by Itoh.[14] However, these compounds undergo intramolecular photodimerization by way of the normal excimer state. Thus, these anthracene systems are not suitable to investigate the interconversion between and interaction in the normal and second excimers, and the extention of the studies to the polymer systems may be more difficult.

No study has been reported so far with respect to the second excimer phenomenon in naphthalene systems (i.e., poly(vinylnaphthalene) and its dimer models). But we thought the second excimer phenomenon more general in condensed aromatic ring compounds than known already and tried to positively make chromophores interact with each other. For this purpose, we prepared poly(vinylnaphthalene) derivatives with methoxy and hydroxy groups[15] on the grounds that we had anticipated that the interaction between these functional groups might have direct effects on the overlapping structure of excimers; the methoxy group is bulky and an electron donor, and the hydrogen group is expected to have a hydrogen bond. In fact, in a previous short communication,[16] we first demonstrated that a second excimer is observed in these dinaphthylpropane derivatives.[17] In the present work, both photostationary and transient measurements are combined in an attempt to unveil their complex photophysical processes, especially from the kinetic point of view.

Experimental Section

Materials. 1,3-Bis(4-methoxy-1-naphthyl)propane (BMNP). 1-Formyl-4-methoxynaphthalene (I) was prepared by stirring a 50-mL methanol solution of CH_3I (2.7 g), K_2CO_3 (4.2 g), and 1-formyl-4-hydroxynaphthalene (II) (5 g) for 4 h at 70 °C in a pressure bottle; II was prepared from 1-naphthol through the Gattermann reaction.[20,21]

On the other hand, 1-acetyl-4-methoxynaphthalene (III) was prepared from 1-methoxynaphthalene through the Friedel–Crafts reaction using CH_3COCl and $AlCl_3$.[22]

I (2.5 g) and III (2.7 g) were added into a 100-mL ethanol solution with NaOH (0.36 g), and dry nitrogen gas was passed through this red solution.[8] The solution was kept stirred overnight while it was tightly stoppered. The yellow precipitate (IV) appeared after 4–5 h (see Scheme I). The precipitate was recrystallized from ethanol; NMR τ 1.1–3.1 (ring, 6), 1.7,2,6 (CH=CH, 1), 5.8 (OCH_3, 3); IR 1650 cm^{-1} (C=O stretching).

A solution of IV (10 g) in 85 mL of tetrahydrofuran distilled beforehand on $LiAlH_4$ was hydrogenated over 2 g of Pd/C, and 1.9 L of H_2 gas was used for this reaction. The solution was evaporated and dried. The product (BMNP) was separated by chromatography on silica gel with *n*-pentane as eluent, and needle-like crystals were obtained by recrystallization from *n*-hexane: mp 78–79 °C; NMR τ 1.4–3.1 (ring, 6), 5.9 (OCH_3, 3), 6.8 ($ArCH_2$, 2), 7.8 (CH_2, 1); IR 1620, 1590, 1510 (ring), 1470, 1390 (CH_3), 1250 (COC) cm^{-1}.

Scheme II

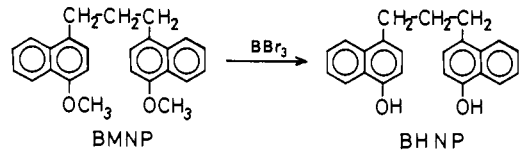

Scheme III

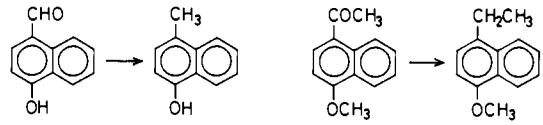

1,3-Bis(4-hydroxy-1-naphthyl)propane (BHNP). A solution of BBr_3 (2 mL) in 20 mL of CH_2Cl_2 was gradually added dropwise into a solution of BMNP (2 g) in 100 mL of CH_2Cl_2 (see Scheme II). After the dropwise addition, the solution was refluxed and stirred overnight; then it was poured into water and the solution was extracted with ether. The ethereal solution was extracted repeatedly with water and then with alkaline aqueous solution. On addition of aqueous solution of hydrochloric acid into this alkaline solution, a precipitate was formed. The colloidal solution was extracted with ether, and the solution was evaporated to dryness. The product was separated by chromatography on silica gel with CH_2Cl_2 as eluent: mp 70–71 °C; NMR τ 1.4–3.2 (ring, 6), 4.6 (OH, 1), 7.0 ($ArCH_2$, 2), 8.1 (CH_2, 1).

Other Products. 1-Hydroxy-4-methylnaphthalene and 1-methoxy-4-ethylnaphthalene were prepared by hydrogeneration of II and III, respectively (see Scheme III).

Sample Solution. All sample solutions were degassed by means of freeze–pump–thaw cycles. Their concentrations were (5×10^{-6})–(1×10^{-5})/M, in which region the fluorescence intensity is in proportion to the concentration and the ratio of the intensities of monomer, normal excimer, and second excimer emissions remains unchanged.

Spectrograde solvents were used without further purification except 2-methyltetrahydrofuran (MTHF), which was distilled on $LiAlH_4$.

Instrumentation. Absorption spectra were measured on a Shimazu MPS-5000 spectrophotometer and fluorescence spectra and fluorescence excitation spectra on a JASCO FP-550 spectrofluorometer. The sample temperature was controlled by an Oxford DN704 cryostat with a DTC-2 digital temperature controller. Temperature regulation is easily better than ±0.5 K; independent temperature measurement was carried out by means of a second thermocouple and a potentiometer. All samples were kept at each set temperature for 30 min to 2 h, and spectra were run repeatedly until perfect duplication was obtained.

Fluorescence lifetimes were measured by the next two different techniques. In the first of the two, the exciting light source was the fourth harmonic, provided by a Quanta-Ray HG-1 harmonic generator, of a Q-switched Quanta-Ray DCR-1 Nd:YAG laser, with a pulse width of 5 ns and maximum power of 30 mJ. The monitoring light intensity was measured with an HTV-R 636 photomultiplier through a grating monochromator (Nikon G-250). The transient signals were recorded by an Iwatsū DM901 digital memory. A single photon counting Ortec-Geos system was used as the second technique. The second harmonics of a Molectron UV24 nitrogen laser and a Molectron DL 14-P dye laser were used as the exciting light sources, with a pulse width of 2 ns and maximum power of 10 mJ. The monitoring light intensity was detected with an HTV-R 1332 photomultiplier through a grating monochromator (Nikon G-250).

Results

Photostationary Results. Figures 1 and 2 show the temperature dependence of the emission spectra of BMNP (1,3-bis(4-methoxy-1-naphthyl)propane) in 2-methyltetrahydrofuran (MTHF). From the difference plot of the degassed emission spectrum and

(13) Hayashi, T.; Suzuki, T.; Mataga, N.; Sakata, Y.; Misumi, S. *Chem. Phys. Lett.* **1976**, *38*, 599.
(14) Itoh, M.; Fuke, K.; Kobayashi, S. *J. Chem. Phys.* **1980**, *72*, 1417.
(15) Itagaki, H.; Okamoto, A.; Horie, K.; Mita, I. *Eur. Polym. J.*, in press.
(16) Itagaki, H.; Obukata, N.; Okamoto, A.; Horie, K.; Mita, I. *Chem. Phys. Lett.* **1981**, *78*, 143.
(17) After our short communication, the second excimer emission of naphthalene chromophore was reported in a poly(1-vinylnaphthalene) system[18] and in a 1-α-naphthyl-3-β-naphthylpropane system.[19]
(18) Gupta, A.; Liang, R.; Moacanin, J.; Kliger, D.; Goldbeck, R.; Horwitz, J.; Miskowski, V. M. *Eur. Polym. J.* **1981**, *17*, 485.
(19) Ito, S.; Yamamoto, M.; Nishijima, Y. *Polym. Preprints, Jpn.* **1981**, *30*, 1316.
(20) Gattermann, L.; Berchelmann, W. *Ber.* **1898**, *31*, 1765.
(21) Adams, R.; Levine, I. *J. Am. Chem. Soc.* **1923**, *45*, 2273.
(22) Gattermann, L.; Ehrhardt, R.; Maisch, H. *Ber.* **1890**, *23*, 1199.

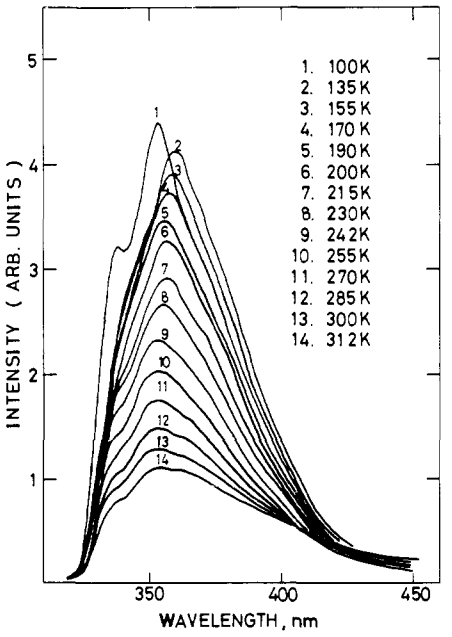

Figure 1. Temperature dependence of the emission spectra of BMNP in MTHF in the temperature region 135–312 K (excitation wavelength 305 nm).

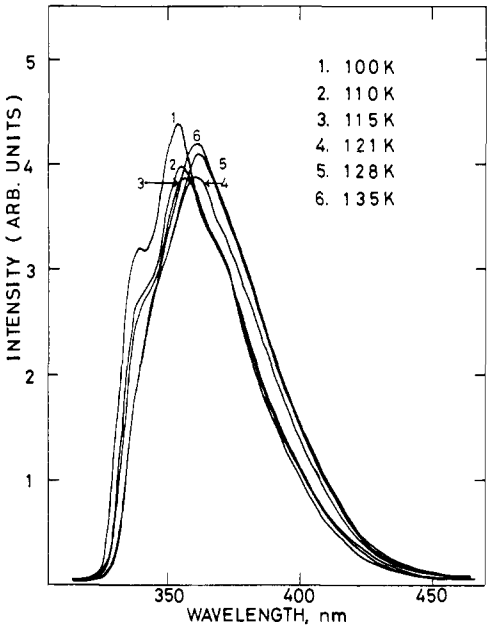

Figure 2. Temperature dependence of the emission spectra of BMNP in MTHF in the temperature region 100–135 K (excitation wavelength 305 nm).

the aerated one (Figure 3), the 340- and 353-nm bands are assigned to the fine structure of the monomer emission, and the broad 410-nm band is assigned to the normal long-lived excimer emission. The emission spectrum of BMNP looks different from that of 1,3-dinaphthylpropane.[8] The latter consists of only a sharp monomer emission peak in the 400–450-nm region. For BMNP in MTHF, aside from the monomer and normal excimer emission bands, another structureless band is perceptible at ca. 370 nm. It looks like a shoulder at room temperature but becomes a pronounced peak as the temperature falls. The fine structure of the monomer emission disappears at low temperatures while it is clear at room temperature. An apparent red shift of the maximum peak in Figure 1 and the disappearance of the fine structure of the monomer emission at 230–120 K can be explained by the appearance and overlap of the structureless peak at ca. 370 nm with the monomer emission peak. Moreover, Figure 2 shows

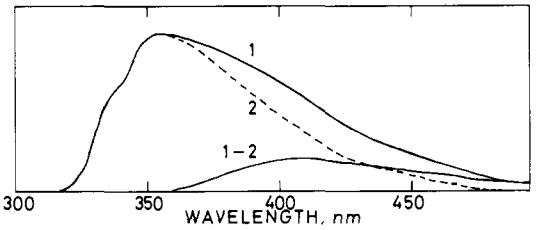

Figure 3. Emission spectra of degassed (1) and aerated (2) solutions of BMNP in ethanol at room temperature (excitation wavelength 305 nm); (1–2) is the difference spectrum of the two normalized ones.

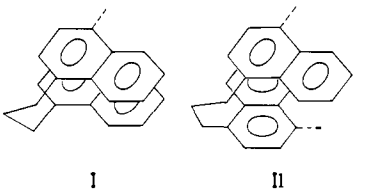

I II

Figure 4. Conformation of the normal excimer (I) and one of the possible models of the second excimer (II).

that the ca. 370-nm peak approaches a maximum near 135 K, and its intensity decreases with further decreasing temperature; thus the 353-nm monomer emission band again becomes a maximum. The existence of a temperature (ca. 140 K) giving a maximum intensity of the second excimer emission has been observed for poly(*N*-vinylcarbazole) (PVCz) in MTHF.[2] In the rigid glass state below 102 K,[4] the emission spectrum consists almost only of monomer fluorescence (i.e., 340 and 353 nm).

The third peak in the 370-nm region for BMNP is assigned to emission from the second excimer having a partly overlapping structure between two aromatic rings, as indicated in Figure 4 (structure II), which is similar to those proposed for dianthrylethane by Mataga,[13] for dianthrylpropane by Itoh,[14] and for PVCz by Itaya.[3] The following facts are taken into account for this conclusion. (1) The difference plot between the emissions of BMNP and its monomer model 1-ethyl-4-methoxynaphthalene shows that there is a peak around 370 nm due to the intramolecular interaction between two aromatic rings in BMNP. (2) The maximum wavelengths of the monomer emission were not influenced much by changing the solvent (333 and 348 nm in nonpolar solvents such as cyclohexane and *n*-hexane, 340 and 353 nm in all other sovlents used). This indicates that the third peak does not come from the red shift of the monomer emission induced by solvent polarity. (3) The fact that the fluorescence excitation spectra for the 370-nm band of BMNP agree well with the absorption spectra and are also similar to those of the monomer model suggests that there is no appreciable interaction between the two naphthalene moieties in ground-state BMNP, and the structure corresponding to this broad band should be formed in the excited state. (4) The 370-nm peak disappears in the rigid glass state at 100 K (for the case in MTHF), showing that the peak is due to dynamic intramolecular interaction between the two aromatic rings, which was also confirmed by the transient experimental data. (5) The intensity of the 370-nm peak increases with decreasing temperature and approaches a maximum near 135 K, which is often observed in many excimer emissions because dissociation can be neglected at low temperatures.[23-25] (6) The rather small Stokes shift of the present excimer fluorescence (3700 cm^{-1}) indicates that the interaction energy between the two naphthyl groups in the excited state is not so large, due to the incomplete overlap of the two moieties.

The three components that constitute an observed fluorescence spectrum of BMNP are estimated in the following way. First, we take for granted that each spectrum of the monomer, second

(23) Birks, J. B. "Photophysics of Aromatic Molecules"; Wiley-Interscience: New York, 1970.
(24) Birks, J. B. *Rep. Prog. Phys.* **1975**, *38*, 975.
(25) Klöpffer, W. In "Organic Molecular Photophysics" Birks, J. B., Ed.; Wiley: New York, 1974.

Table I. Coefficients of Eq 1 Obtained from the Emission Spectra of BMNP in MTHF (Figure 1)

coeff	temp region, K	equation	values obtained	av
$r^{D_2}_{353}$	145-190	$(I_{353} - I_0^M)/(I_{370} - 0.74I_0^M)$	0.403, 0.415, 0.407, 0.406	0.41
$r^{D_1}_{353}$		[a]		0
r^{M}_{370}	255-312	$\{I_{370} - 0.53(I_{410} - I_0^M)\}/I_0^M$	0.733, 0.743, 0.745, 0.747, 0.775	0.74
$r^{D_1}_{370}$		[a]	0.524, 0.535	0.53
r^{M}_{410}		[a]		0.14
$r^{D_2}_{410}$	121-155	$(I_{410} - 0.14I_0^M)/(I_{370} - 0.74I_0^M)$	0.393, 0.386, 0.380, 0.378	0.38
r^{M}_{353}	270-312, 77-110	I_{340}/I_0^M	0.735, 0.727, 0.735, 0.729, 0.725, 0.729, 0.715	0.73

[a] See the text.

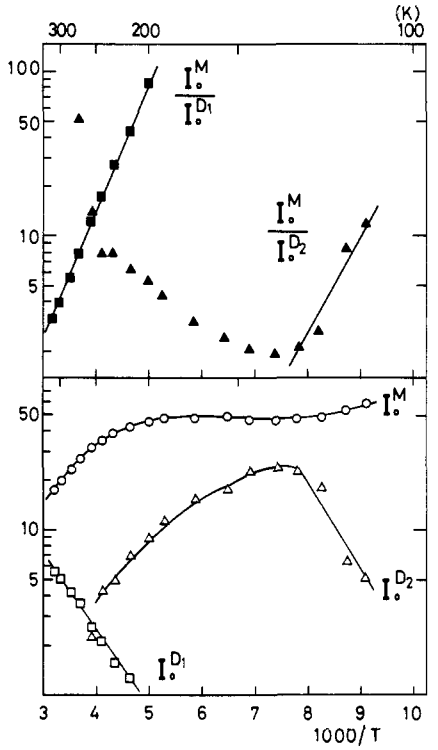

Figure 5. Estimated intensity values of each of the components, I_0^M (○), $I_0^{D_1}$ (□), and $I_0^{D_2}$ (△), and their ratios, $I_0^M/I_0^{D_1}$ (■) and $I_0^M/I_0^{D_2}$ (▲), from the emission spectra of BMNP in MTHF.

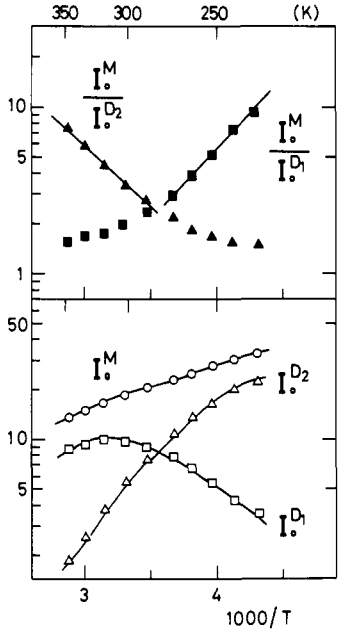

Figure 6. Estimated intensity values of each of the components, I_0^M (○), $I_0^{D_1}$ (□), and $I_0^{D_2}$ (△), and their ratios, $I_0^M/I_0^{D_1}$ (■) and $I_0^M/I_0^{D_2}$ (▲), from the emission spectra of BMNP in acetonitrile.

excimer, and normal excimer has the same peak wavelength at any temperature; this treatment has been done in several papers.[1-3] In fact, the fine structure of the monomer emission observed at 340 and 353 nm at room temperature reappears below 100 K, where the solution is in the rigid glass state and the motion of the rings is limited. And the difference plot of the degassed emission spectrum and aerated one at 255 K also peaks at 410 nm as well as (see Figure 3) at 300 K. Second, the maximum wavelengths of the normal excimer and the second excimer are taken as 410 nm and 370 nm, respectively.

The following equations (eq 1) hold in which M, D_1, and D_2

$$I_{353} = I_0^M + r_{353}^{D_2} I_0^{D_2} + r_{353}^{D_1} I_0^{D_1}$$
$$I_{370} = r_{370}^{M} I_0^M + I_0^{D_2} + r_{370}^{D_1} I_0^{D_1} \quad (1)$$
$$I_{410} = r_{410}^{M} I_0^M + r_{410}^{D_2} I_0^{D_2} + I_0^{D_1} \qquad I_{340} = r_{353}^{M} I_0^M$$

mean the excited monomer state, the normal excimer state, and the second excimer state, respectively, I means the observed emission intensity at respective wavelength, I_0^x (x: M, D_1, D_2) is the peak intensity of each species, and the coefficients r_y^x (y: wavelength) are the relative intensities of each components at respective wavelength y.

The values of the coefficients obtained from analysis of the curves (Figures 1 and 2) are shown in Table I. The values of $r_{353}^{D_1}$ and $r_{370}^{D_1}$ were obtained from the room-temperature spectrum of the normal excimer obtained as a difference plot of a degassed emission curve and an aerated one (Figure 3), as well as from the difference plot of a degassed fluorescence spectra at room temperature and one in the rigid glass state. The value of r_{410}^{M} was obtained from the emission spectra in the rigid glass state. Other values obtained from each equation are shown in Table I.

Figures 5 and 6 show the temperature dependence of the calculated values of I_0^x and their ratios obtained by using the above parameters. Various activation energies to be mentioned in Discussion II were obtained from the slopes of their ratios.

Transient Emission Spectra. Typical emission response curves for a dilute solution of BMNP in tetrahydrofuran (THF) are shown in Figures 7 and 8. At room temperature, the emission at 350 nm (Figure 7) is due almost exclusively to the monomer and second excimer, and the emission at 470 nm (Figure 8) only to the normal excimer, which was confirmed by the difference spectra.

All decay curves detected at any wavelength give only the same three decay constants, as shown in Figure 9 and Table II, corresponding to the existence of three excited states interacting with one another. If these three decay constants are denoted by λ_1, λ_2, and λ_3 ($\lambda_3 > \lambda_2 > \lambda_1 > 0$), the emission intensity of each excited state decays according to eq 2, where t is time.

$$I(t) = \sum_{i=1}^{3} A_i \exp(-\lambda_i t) \quad (2)$$

The decay constants for Figure 7 were obtained in the following way: the smallest decay constant (λ_1) (i.e., the longest time constant) was not observed within this time range, probably because of the overlapping of the second excimer emission and/or the very small value of the preexponential term of λ_1. So first the middle decay constant (λ_2) was determined by a least-squares method from the linear part of the semilogarithmic plots between 50 and 150 ns; second, by the subtraction of the extrapolated value

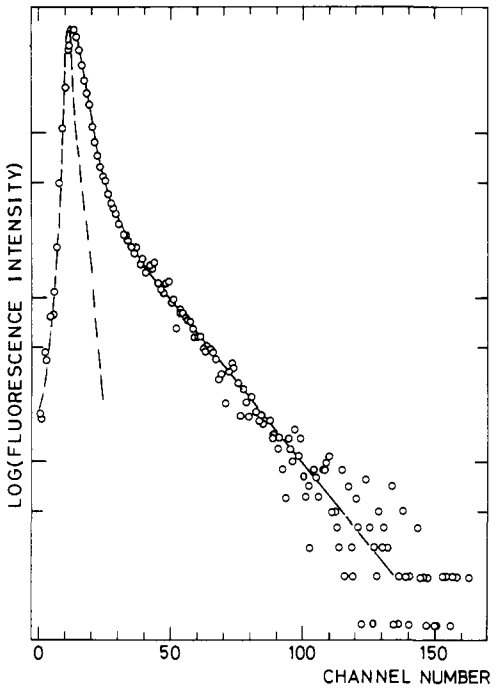

Figure 7. Fluorescence decay curve of BMNP in THF observed at 350 nm (O) and the excitation lump (broken line) at room temperature; 1 channel = 1.06 ns. The solid line shows the theoretical decay curve (see III under Discussion).

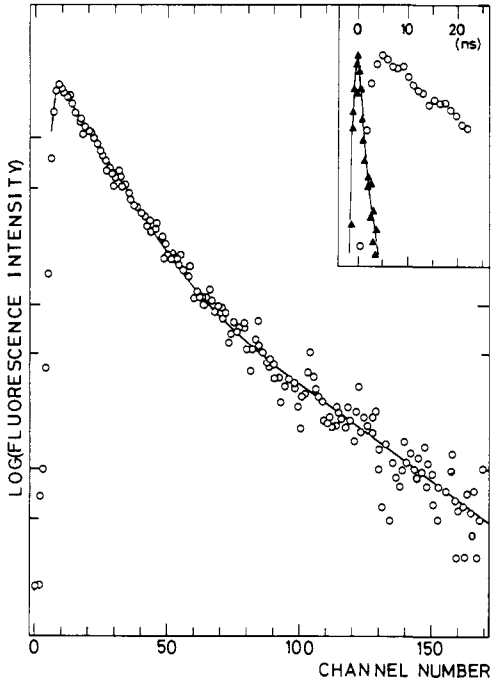

Figure 8. Fluorescence decay curve of BMNP in THF observed at 470 nm (O) and the excitation lump (▲) at room temperature; 1 channel = 2.12 ns. The solid line shows the theoretical decay curve (see III under Discussion).

of the linear part from the decay curve, the largest decay constant (λ_3) was determined between 0 and 50 ns. The rise curve of Figure 7 agrees with the excitation pulse. The pulse width is 5 ns for the Nd:YAG laser and 2 ns for the N_2-dye laser. So the shortest time constant (the largest decay constant) is barely measurable, and we could indicate that the largest decay constants are in the region of the values shown in Table II. Calculated decay curves with the values given in Table II are shown by a solid line in Figures 7 and 8.

A value of 4 ns is very small as the singlet lifetime of naphthalene moieties. However, it is generally known that introduction of a methoxy group reduces the singlet lifetime of compounds. For example, the singlet lifetime of 1-methoxynaphthalene in methanol is 18 ns, while that of naphthalene in methanol is 74.7 ns.[26] Moreover, considering that there exist two excimer formation paths escaping from the excited monomer state in addition to radiative and nonradiative deactivation processes, this value would be reasonable.[27]

Table II. Decay Constants in Several Solvents at Room Temperature

solvent	$\lambda_1 \times 10^7$, s^{-1}	$1/\lambda_1$, ns	$\lambda_2 \times 10^7$, s^{-1}	$1/\lambda_2$, ns	$\lambda_3 \times 10^7$, s^{-1}	$1/\lambda_3$, ns
ethanol	1.4	70	4.4	23	30	3.3
THF	1.3	80	4.5	22	25	4.0
cyclohexane	1.1	88	4.9	20	24	4.1

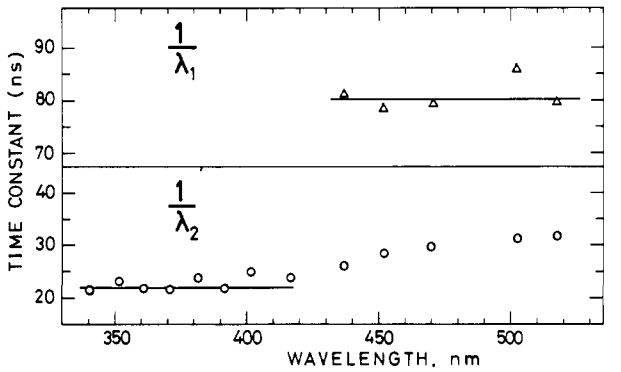

Figure 9. Wavelength dependence of the decay constants λ_1 and λ_2 of BMNP in THF at room temperature.

Next we will examine Figure 8, which shows the decay curve of only the normal excimer. The decay constants in Figure 8 were obtained in the following way: first, the smallest decay constant (λ_1) was determined by a least-squares method from the linear part of the semilogarithmic plots between 150 and 400 ns; second, by the subtraction of the extrapolated value of the linear part from the decay curve, we obtained the middle decay constant (λ_2) between 30 and 150 ns. The shortest time constant (ca. 4 ns) cannot be obtained quantitatively in Figure 8, since the shortest time constant term, $A_3 \exp(-\lambda_3 t)$, acts as a rise term. In fact, as the insert in Figure 8 shows, the rise peak is observed clearly 4–5 ns after the excitation pulse peak. Therefore it is concluded that the emission of the normal excimer decays double exponentially with the time constants, 20 and 80 ns, and shows a rise curve at the earliest region. These facts indicate that the normal excimer decays according to eq 3, where the reciprocal of λ_i is

$$I_{D_1}(t) = (+)\exp(-\lambda_1 t) + (+)\exp(-\lambda_2 t) + (-)\exp(-\lambda_3 t) \quad (3)$$

4 (λ_3^{-1}), 20 (λ_2^{-1}), and 80 ns (λ_1^{-1}). The symbols (+) and (−) mean that the coefficient of each term has a positive or negative sign. We will discuss the kinetic scheme of BMNP to examine whether or not the calculated decay pattern of the normal excimer emission under an assumed kinetic scheme agrees with eq 3.

Figure 9 shows that the observed middle time constants, $1/\lambda_2$ (20 ns), apparently increase in proportion as the response wavelength, y, changes from 400 to 450 nm and become almost constant for longer wavelengths. This would be explained by the change in the sign of the largest decay constant term [$\exp(-\lambda_3 t)$] from (+) for y = 350–400 nm to (−) for y > 450 nm, due to the decrease in contribution of monomer emission to the decay curve.

The decay constants were found to change with solvents as shown in Table II. The smallest decay constant, λ_1, increases as the solvent polarity increases.

(26) Hermann, V. H.; Koltzenburg, G.; Schulte-Frohlinde, D. *Ber. Bunsenges. Phys. Chem.* **1973**, *77*, 677.
(27) Quina, F. H.; Hamlet, Z.; Carroll, F. A. *J. Am. Chem. Soc.* **1977**, *99*, 2240.

Discussion

I. Determination of the Kinetic Scheme. The kinetic scheme appropriate for description of a system with two intrachain excimer states is given in eq 4, where M, D_1, and D_2 represent an excited

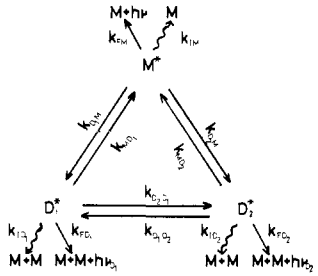

(4)

monomeric chromophore, a normal excimer, and a second excimer, respectively. The notation of various rate constants follows that of Birks,[23] in which the subscripts F and I mean radiative and nonradiative deactivations of excited states. The nonradiative deactivation processes include both internal conversion and intersystem crossing. The rate constants k_{MD_1} and k_{MD_2} are those for dissociation of the two excimers to yield an excited monomer while $k_{D_1D_2}$ is that for direct conversion of D_2 to D_1. The processes for k_{D_1M} and k_{D_2M} involve conformational changes to meet the geometrical requirement necessary for each respective excimer, probably with diffusion-controlled rates. In our experimental conditions (10^{-6} M), the intermolecular excimer can be disregarded. Therefore, k_{D_1M} and k_{D_2M} represent only the process for intramolecular excimer formation.

The values of all three emissions, I_M, I_{D_1}, and I_{D_2}, decay in a complex manner becuase they are the sum or difference of three exponentials with different decay constants λ_1, λ_2, and λ_3:

$$\lambda_3 > \lambda_2 > \lambda_1 > 0 \tag{5}$$

each of which contains all the rate constants (see Appendix).

The general scheme given by eq 4 will be modified for special cases. Let us consider two simplified models: (i) the case where one excimer state is an intermediate to another—as D_1 has a perfect overlapping structure and is more stable than D_2 by resonance energy, we may discard the case in which D_1 is an intermediate to D_2, so eq 6 holds:

$$M^* \rightleftarrows D^*_2 \rightleftarrows D^*_1 \qquad k_{D_1M} = 0 \tag{6}$$

(ii) the case where the formation of two excimers is independent of each other—in this case, each excimer may have a large binding energy, and the potential barrier between D_1 and D_2 is large; this corresponds to eq 7:

$$D^*_1 \rightleftarrows M^* \rightleftarrows D^*_2 \qquad k_{D_1D_2} = k_{D_2D_1} = 0 \tag{7}$$

From the analysis of the experimental curves, we will be able to judge which model fits better to our system.

In case i, k_{D_1M} is equal to zero. Under the conditions that there should exist three different excited states and $k_{D_1M} = 0$, we can calculate each preexponential term A_i of eq 2 and estimate whether each A_i has a positive or negative sign. Actually, as is shown in the Appendix, we obtain eq 8 under these conditions. As shown

$$I_M(t) = (+)\exp(-\lambda_1 t) + (+)\exp(-\lambda_2 t) + (+)\exp(\lambda_3 t)$$

$$I_{D_1}(t) = (+)\exp(-\lambda_1 t) + (-)\exp(-\lambda_2 t) + (+)\exp(-\lambda_3 t)$$

$$I_{D_2}(t) = (+)\exp(-\lambda_1 t) + (+)\exp(-\lambda_2 t) + (-)\exp(-\lambda_3 t) \tag{8}$$

already in the section of transient results, the experimental $I_{D_1}(t)$ decays according to eq 3, which differs from the theoretical one (eq 8) on the basis of the assumption that $k_{D_1M} = 0$. This demonstrates that case i can be denied.

Next let us consider another simplified case, case ii. In this case, $k_{D_1D_2} = k_{D_2D_1} = 0$ holds and eq A9 in the Appendix will be obtained for each fluorescence response function. For determination of the signs of each term in eq A9, two cases corresponding to the next alternative inequalities,

$$\lambda_3 > k_{FD_1} + k_{ID_1} + k_{MD_1} > \lambda_2 > k_{FD_2} + k_{ID_2} + k_{MD_2} > \lambda_1 > 0 \tag{9}$$

or

$$\lambda_3 > k_{FD_2} + k_{ID_2} + k_{MD_2} > \lambda_2 > k_{FD_1} + k_{ID_1} + k_{MD_1} > \lambda_1 > 0 \tag{10}$$

should be considered. In the case of inequality 9, we obtain eq 11, and in the case of inequality 10, we obtain eq 12 for the D_1

$$I_M(t) = (+)\exp(-\lambda_1 t) + (+)\exp(-\lambda_2 t) + (+)\exp(-\lambda_3 t) \tag{11a}$$

$$I_{D_1}(t) = (+)\exp(-\lambda_1 t) + (+)\exp(-\lambda_2 t) + (-)\exp(-\lambda_3 t) \tag{11b}$$

$$I_{D_1}(t) = (+)\exp(-\lambda_1 t) + (-)\exp(-\lambda_2 t) + (-)\exp(-\lambda_3 t) \tag{12}$$

fluorescence response function. Equation 11b fits the experimental pattern (eq 3). This means that the experimental results do not contradict the scheme $k_{D_1D_2} = k_{D_2D_1} = 0$ (eq 7), with the condition of inequality 9.

Of course the above scheme represents only one of the possible mechanisms. We will examine it in more detailed manner. We can infer that $k_{D_2D_1}$ is sufficiently small compared with other rate constants because, in general, the normal excimer state is more stable than the second excimer state from the consideration of resonance energy. The possibility that the less stable second excimer is formed from the normal excimer staying in a stable energy level is very small.

Now we need to examine whether or not $k_{D_1D_2}$ is very small. At room temperature, the intensity of the second excimer is very weak, while at low temperature it is very strong (Figures 5 and 6). Two explanations are possible: (a) $k_{D_1D_2}$ is very large, and once the second excimer is formed, it quickly turns to the normal excimer. And as the temperature decreases, $k_{D_1D_2}$ decreases, the second excimer state turns to be more stable, and its intensity increases ($k_{D_1D_2} \gg k_{MD_2}$). (b) k_{MD_2} is very large at room temperature, and once the second excimer is formed, it quickly dissociates to the excited monomer and ground-state monomer; therefore, its intensity is very weak. As the temperature decreases, k_{MD_2} decreases, the second excimer state becomes more stable, and its intensity increases ($k_{MD_2} \gg k_{D_1D_2}$).

As the radiative rate constant k_{FD_2} is supposed to be similar to k_{FD_1}, it becomes a serious problem regarding which of the processes a or b is valid. However, the assumption that k_{MD_2} may be very small is very questionable, because the increase of the emission intensity of the second excimer does not correspond to the decrease of that of the normal excimer at low temperatures (see Figures 5 and 6). The second excimer emission increases at the low-temperature region until 135 K, which means that the abundant second excimer state is formed. Figures 5 and 6 show that the normal excimer emission approaches near zero below 200 K. If $E_{D_1D_2}$ were very small, the normal excimer emission would not decrease so much. And if $k_{D_1D_2}$ were very large, the second excimer emission should have a maximum value at the higher temperature than the normal excimer emission approaches near zero. (See Figure 5.) Therefore case b holds in our system.

So the temperature dependence of the second excimer emission is explained by the decrease of the dissociation rate constant k_{MD_2} with decreasing temperature. It will prove that the binding energy for the second excimer formation, $-\Delta H_2 = E_{MD_2} - E_{D_2M}$, is small in the next section.

From the arguments given above, we could show that each excimer is formed directly from the excited monomer and the ground-state monomer, and k_{MD_2} cannot be neglected at room temperature. Moreover, we could show that the experimental decay curves corresponds to the theoretical ones, which assume that $k_{D_1D_2}$ and $k_{D_2D_1}$ is very small compared with other rate constants.

II. Activation Energies from Photostationary Data. We have

discussed the kinetic scheme of this experimental system from transient data. Now we calculate some activation energies according to the scheme of eq 7.

First we will consider the general case (eq 4). The analysis of the photostationary kinetics with steady-state approximation gives the intensity of each components.

$$I_o^M = k_{FM}[M^*] = \frac{k_{FM}(BC - k_{D_1D_2}k_{D_2D_1})}{H} I \quad (13)$$

$$I_o^{D_1} = k_{FD_1}[D_1^*] = \frac{k_{FD_1}(k_{D_1M}C + k_{D_1D_2}k_{D_2M})}{H} I \quad (14)$$

$$I_o^{D_2} = k_{FD_2}[D_2^*] = \frac{k_{FD_2}(k_{D_2M}B + k_{D_2D_1}k_{D_1M})}{H} I \quad (15)$$

$$H = ABC - k_{D_1D_2}k_{D_2D_1}A - k_{D_2M}k_{MD_2}B - k_{D_1M}k_{MD_1}C - k_{D_1M}k_{MD_2}k_{D_2D_1} - k_{D_2M}k_{MD_1}k_{D_1D_2} \quad (16)$$

where

$$A = k_{FM} + k_{1M} + k_{D_1M} + k_{D_2M}$$
$$B = k_{FD_1} + k_{1D_1} + k_{MD_1} + k_{D_2D_1} \quad (17)$$
$$C = k_{FD_2} + k_{1D_2} + k_{MD_2} + k_{D_1D_2}$$

As $k_{D_1D_2} = k_{D_2D_1} = 0$ for our system (eq 7), each of the above equations is simplified due to the disappearance of the second term.

Three distinct temperature regions are considered. Region I corresponds to the very low temperatures from 100 to 135 K. As seen in Figure 5, increasing temperature leads to an increase in the second excimer fluorescence, and it has the maximum value at 135 K. Within this temperature region, the intensity of the normal excimer fluorescence is nearly zero. Then the following approximations are valid in this region: first, the rate constants from the D_1 state are negligible, and second, the thermal dissociation of D_2 is negligible, i.e., $k_{MD_2} = 0$.

The nonradiative deactivation of the second excimer, k_{1D_2}, is supposed to consist of two terms[23] as

$$k_{1D_2} = k^0_{1D_2} + k'_{1D_2} \exp(-E_{1D_2}/RT) \quad (18)$$

We assume that k_{1D_2} is equal to $k^0_{1D_2}$ (temperature-independent term); i.e., $k^0_{1D_2} \gg k'_{1D_2} \exp(-E_{1D_2}/RT)$ for region I.

Then we can express the intensity ratio of the monomer fluorescence to second excimer fluorescence as

$$\frac{I_o^M}{I_o^{D_2}} = \frac{k_{FM}(k_{FD_2} + k_{1D_2})}{k_{FD_2}k_{D_2M}} \quad (19)$$

k_{FM} and k_{FD_2} are supposed to be independent of temperature,[23] so that the temperature-dependent term of eq 19 is only k_{D_2M}; thus a plot of ln $(I_o^M/I_o^{D_2})$ vs. $1/T$ should yield the activation energy E_{D_2M}. Figure 5 gives a value of $E_{D_2M} = 3.0$ kcal/mol.

In this temperature region, $k_{D_1M}k_{MD_1}$ can be neglected; thus eq 16 can be reduced to

$$H = ABC - k_{D_2M}k_{MD_2}B$$

Therefore we can obtain the next formula.

$$I_o^{D_2} = \frac{k_{FD_2}k_{D_2M}B}{ABC - k_{D_2M}k_{MD_2}B} = \frac{k_{FD_2}k_{D_2M}}{AC - k_{D_2M}k_{MD_2}}$$

It is supposed that $k_{1M} = k^0_{1M}$ (temperature-independent term) holds at the low-temeprature region,[23] and $k_{D_2M}k_{MD_2}$ can be disregarded in comparison with the first term; thus

$$I_o^{D_2} = \frac{k_{FD_2}k_{D_2M}}{(k_{FM} + k^0_{1M})(k_{FD_2} + k^0_{1D_2})} \quad (20)$$

k_{D_2M} is the only temperature-dependent term in eq 20; therefore a plot of ln $(I_o^{D_2})$ vs. $1/T$ would also yield the activation energy E_{D_2M}. Figure 5 actually gave a value of $E_{D_2M} = 2.7$ kcal/mol. This means that the above assumption is appropriate.

Temperature region II corresponds to temperatures from 150 up to 230 K (below 230 K acetonitrile solution is frozen). We estimate E_{1D_2} as follows. In this region, the rate constants from the D_1 state are negligible, and the thermal dissociation of D_2 is also negligible; i.e., $k_{MD2} = 0$. Therefore eq 21 is valid. The

$$I_o^{D_2} = \frac{k_{FD_2}k_{D_2M}}{(k_{FM} + k^0_{1M})(k_{FD_2} + k^0_{1D_2} + k'_{1D_2} \exp(-E_{1D_2}/RT))} \quad (21)$$

intensity of the second excimer emission has the maximum value, $I_{D_2}^{max}$, at 135 K. We can approximate below this temperature $k_{1D_2} = k^0_{1D_2}$ (see eq 18). Then

$$I_{D_2}^{max} = \frac{k_{FD_2}k_{D_2M}}{(k_{FM} + k^0_{1M})(k_{FD_2} + k^0_{1D_2})} \quad (20')$$

The k_{D_2M} is supposed to be of the form

$$k_{D_2M} = k'_{D_2M} \exp(-E_{D_2M}/RT) \quad (22)$$

Then from eq 20', 21, and 22 we can obtain

$$\frac{1}{I_o^{D_2}} = \frac{(k_{FM} + k^0_{1M})(k_{FD_2} + k^0_{1D_2})}{k_{FD_2}k_{D_2M}} + \frac{(k_{FM} + k^0_{1M})k'_{1D_2} \exp(-E_{1D_2}/RT)}{k_{FD_2}k'_{D_2M} \exp(-E_{D_2M}/RT)} = \frac{1}{I_{D_2}^{max}} + \frac{(k_{FM} + k^0_{1M})k'_{1D_2} \exp[-(E_{1D_2} - E_{D_2M})/RT]}{k_{FD_2}k'_{D_2M}}$$

Therefore

$$\frac{I_{D_2}^{max}}{I_o^{D_2}} - 1 = \frac{I_{D_2}^{max}(k_{FM} + k^0_{1M})k'_{1D_2}}{k_{FD_2}k'_{D_2M}} \exp[-(E_{1D_2} - E_{D_2M})/RT] \quad (23)$$

Of course, when $I_{D_2}^{max}(k_{FM} + k^0_{1M})k'_{1D_2}/k_{FD_2}k'_{D_2M}$ is constant, then a plot of ln $(I_{D_2}^{max}/I_o^{D_2} - 1)$ vs. $1/T$ should yield the difference of two activation energies. Actually this has been done as shown in Figure 10 and from this linearity, a value of $(E_{1D_2} - E_{D_2M}) = 2.6$ kcal/mol was determined. From this value, we get $E_{1D_2} = E_{D_2M} + 2.6 = 5.6$ kcal/mol. As to E_{1D_1}, the nonradiative deactivation energy of the normal excimer, the following values are known: e.g., 6 kcal/mol for poly(1-vinylnaphthalene),[28] 12 kcal/mol for 1,3-bis(1-naphthyl)propane,[8] 6.7 kcal/mol for 1-methylnaphthalene.[29] The value of 5.6 kcal/mol for E_{1D_2} is consistent with these values for E_{1D_1}.

Temperature region III appears from 250 up to 320 K in MTHF and from 230 up to 285 K in acetonitrile. In this temperature region, the intensity of the normal excimer emission increases with increasing temperature, while the intensity of the second excimer emission approaches zero. First we will consider the intensity ratio of monomer fluorescence to the normal excimer fluorescence.

$$\frac{I_o^M}{I_o^{D_1}} = \frac{k_{FM}(k_{FD_1} + k_{1D_1} + k_{MD_1})}{k_{FD_1}k_{D_1M}} \quad (24)$$

As k_{FM} and k_{FD_1} are independent of temperature,[23] the temperature-dependent terms in eq 24 are k_{D_1M}, k_{1D_1}, and k_{MD_1}. Now we assume that the thermal deactivation process is not competing with fluorescence; $k_{FD_1} \gg k_{1D_1}$. This assumption was also used by Chandross and Dempster.[8] If $k_{FD_1} >> k_{MD_1}$ is valid, eq 24 can be reduced to eq 25. Nishijima et al.[30] reported the tem-

$$\frac{I_o^M}{I_o^{D_1}} = (\text{constant})\frac{1}{k_{D_1M}} \quad (25)$$

(28) David, C.; Piens, M.; Geuskens, G. *Eur. Polym. J.* **1976**, *12*, 621.
(29) Cundall, R. B.; Pereira, L. C. *Chem. Phys. Lett.* **1972**, *15*, 383.
(30) Ito, S.; Yamamoto, M.; Nishijima, Y. *Rep. Prog. Polym. Phys. Jpn.* **1976**, *19*, 421.

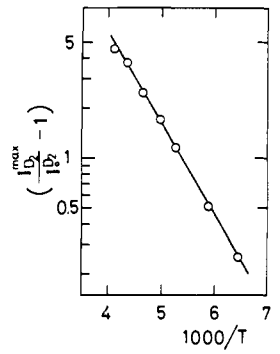

Figure 10. Temperature dependence of ln $(I_{D_2}^{max}/I_o^{D_2} - 1)$ in MTHF.

perature dependence of k_{MD_1} of poly(2-vinylnaphthalene) (P2VN) and bis(2-naphthyl)propane (B2NP): 8×10^6 s^{-1} (300 K) and 2×10^4 s^{-1} (250 K) for P2VN; 1×10^7 s^{-1} (300 K) and 2×10^6 s^{-1} (250 K) for B2NP. David et al.[28] reported that $k_{FD_1} + k^0_{ID_1}$ of poly(1-vinylnaphthalene) is about 1×10^7 s^{-1}. Unless k_{MD_1} is negligible, a plot of ln $(I_o^M/I_o^{D_1})$ vs. $1/T$ ought to have deviated from a straight line due to its complicated temperature dependence. However, Figures 5 and 6 show that this plot gives essentially a straight line. This fact indicates that eq 25 is valid. A plot of ln $(I_o^M/I_o^{D_1})$ vs. $1/T$ gives a value of $E_{D_1M} = 3.8$ kcal/mol in MTHF and 3.7 kcal/mol in acetonitrile. While this plot in acetonitrile gives a straight line between 285 and 230 K, it loses its linearity above 285 K. This behavior can be explained by the increase of k_{MD_1}, because in the high-temeprature region the excimer formation is generally known to attain a dynamic equilibrium.[23]

Next we estimate the binding energy $(E_{MD_2} - E_{D_2M})$ of the second excimer for region III as follows. From eq 13 and 15, we obtain the following:

$$\frac{I_o^M}{I_o^{D_2}} = \frac{k_{FM}(k_{FD_2} + k_{ID_2} + k_{MD_2})}{k_{FD_2}k_{D_2M}} \tag{26}$$

k_{FM} and k_{FD_2} are assumed to be independent of temperature.[23] k_{ID_2} is supposed to be of the form as in eq 18, and the second temperature-dependent term of eq 18 cannot be disregarded in this temperature region. From the transient data, k_{MD_2} is thought to be large at room temperature (I under Discussion). Then we assume that $k_{MD_2} \gg k_{FD_2}$, k_{ID_2} is valid. Equation 27 can be obtained under this assumption. If this assumption were not valid,

$$\frac{I_o^M}{I_o^{D_2}} = (\text{constant})\frac{k_{MD_2}}{k_{D_2M}} \tag{27}$$

a plot of ln $(I_o^M/I_o^{D_2})$ vs. $1/T$ should have lost its linearity. A plot of this ratio vs. $1/T$ of BMNP in acetonitrile (Figure 6) gives essentially a straight line and a value of $(E_{MD_2} - E_{D_2M}) = -\Delta H_2 = 3.1$ kcal/mol. The calculated values for activation and binding energies are shown in Table III.

A few comments are given about the activation energies obtained above. With regard to the activation energy for the second excimer formation, E_{D_2M}, the following values are reported: 2.4 kcal/mol for poly(*N*-vinylcarbazole) (PVCz)[1] and 1.9 kcal/mol for dianthrylethane.[31] These values are smaller than activation energies for the normal excimer formation (e.g., $E_{D_1M} = 4.0$ kcal/mol for PVCz[1]), or in other words, they are smaller than the rotational barrier required for forming the perfectly overlapping structure of two aromatic rings. In our experimental system, E_{D_2M} is ca. 3 kcal/mol while E_{D_1M} is 3.8 kcal/mol, and these results are consistent with the reported values. Figure 8 shows the conformation of the normal excimer and one of the possible models of the second excimer. The difference in activation energies for two kinds of excimer formation would be probably caused by the difference in the rotational barrier in a methylene chain, and one of the possible models of second excimer was shown in Figure 4.

Table III. Values of Activation Energies of BMNP in MTHF and in Acetonitrile (kcal/mol)

solvent	E_{D_1M}	E_{D_2M}	E_{ID_2}	$-\Delta H_2$
MTHF	3.8	3.0	5.6	
acetonitrile	3.7			3.1

We obtained the binding energy of the second excimer $-\Delta H_2 = (E_{MD_2} - E_{D_2M}) = 3.1$ kcal/mol (in acetonitrile). This value is smaller than that of the intramolecular normal excimer so far reported: $-\Delta H_1 = 6.9$ kcal/mol (P1VN), 6.5 kcal/mol (P2VN), and 8.3 kcal/mol (polystyrene);[32] 6.0 kcal/mol (1,3-bis(4-biphenyl)propane).[33] The smaller value of the binding energy, $-\Delta H_2$, compared with $-\Delta H_1$ would be one of the possible reasons why the second excimer phenomena have not been found generally, whereas the activation energy for the second excimer formation, E_{D_2M}, is smaller than that of the normal excimer formation, E_{D_1M}.

The excimer formation process is supposed to be determined by two factors: one is that two chromophores are brought into a sandwich arrangement against a bulky repulsion force, and another is the stabilization by the π-electronic resonance between two chromophores. The perfect overlapping structure cannot be formed until the two rings overcome the steric hindrance, but this structure is stabilized by the large resonance energy. Conversely the partially overlapping structure of the second excimer can be formed more easily because of the smaller repulsion force; however, it cannot be stabilized much, so it easily dissociates. Whether an aromatic compound shows the second excimer fluorescence or not is probably due to both its steric hindrance and π-electronic resonance energy. And in the case of BMNP, the introduction of a methoxy group, which is the typical electron donor, may enhance the resonance energy of the second excimer state; however, $-\Delta H_2$ (i.e., binding energy) = 3.1 kcal/mol is still smaller than that of the normal excimer.

In regard to the second excimer phenomenon, further investigation will be necessary on the stabilization of electronic resonance and its conformational steric hindrance.

III. Estimation of Some Rate Constants. It is difficult to exactly calculate each rate constant. However, if eq 7 is valid, we can estimate *A*, *B*, and *C*, shown in eq 17. Under the assumption of eq 7, the decay curve of the normal excimer obeys eq A9b. The values of λ_1, λ_2, and λ_3 can be obtained from the experimental results; then the only unknown quantity necessary to draw the theoretical decay curve of relative intensity according to A9b is *C*. We can estimate *C* by curve fitting with the experimental results, as given in Figure 8 in THF measured at 470 nm, where the fluorescence comes only from the normal excimer.

The above simulation is done under the conditions of inequality 9, and *C* is estimated to be ca. 1.8×10^7 s^{-1}, a value near λ_1.

When *C* is 1.8×10^7 s^{-1}, we can further estimate *B* from the monomer emission decay curve shown by eq A9a. Of course the experimental results, for instance Figure 7, do not show only the monomer emission because the second excimer emission overlaps in this wavelength region. However, Figures 5 and 6 show that the intensity of monomer emission is larger than that of second excimer emission at room temperature; then we invoked the assumption that Figure 7 would show the $\exp(-\lambda_2 t)$ and $\exp(-\lambda_3 t)$ terms of the monomer emission decay curve. By curve fitting under this assumption, we found *B* to be very close to λ_2, and *B* was determined to be about 5×10^7 s^{-1} in THF.

Next from eq A3 (see Appendix), if

$$\lambda_1 + \lambda_2 + \lambda_3 = A + B + C$$

is valid, then we can calculate *A* as 2×10^8 s^{-1}. The calculated values are summarized in Table IV.

(31) Hayashi, T.; Suzuki, T.; Mataga, N.; Sakata, Y.; Misumi, S. *J. Phys. Chem.* **1977**, *81*, 420.

(32) Fox, R. B.; Price, T. R.; Cozzens, R. F.; McDonald, J. R. *J. Chem. Phys.* **1972**, *57*, 534.

(33) Zachariasse, K. A.; Kühnle, W.; Weller, A. *Chem. Phys. Lett.* **1978**, *59*, 375.

Table IV. Estimated Rate Constants (s^{-1}) of BMNP in THF at Room Temperature

$k_{MD_1} + k_{FD_1} + k_{ID_1}$	$k_{MD_2} + k_{FD_2} + k_{ID_2}$	$k_{D_1M} + k_{D_2M} + k_{FM} + k_{IM}$
5×10^7	1.8×10^7	2×10^8

These values may have large errors. But they demonstrate the tendency that B and C are close to λ_2 and λ_1, respectively, while A is about 10^8, and this value is much larger than B and C. At room temperature, C is composed of k_{MD_2}, k_{FD_2}, and k_{ID_2}, while B is composed of k_{MD_1}, k_{FD_1}, and k_{ID_1}. That the sum of these rate constants is 10^7 is not extraordinary. In the relation $A = k_{FM} + k_{IM} + k_{D_1M} + k_{D_2M}$ (eq 17), the two excimer formation rate constants k_{D_1M} and k_{D_2M}, and the radiation rate constant of monomer emission, k_{FM}, would be reasonably large.

Acknowledgment. We are very grateful to Professor Saburo Nagakura and especially to Dr. Junko Nakamura at the Institute of Physical and Chemical Research for helping us to measure the decay curve and to Professor Shigeo Nishimura at Tokyo University of Agriculture and Technology for kindly providing the apparatus and the efforts for hydrogenation.

Appendix

The kinetic treatment of eq 4 in detail is as follows. The general rate equations are given in eq A1.

$$d[M^*]/dt = I - (k_{FM} + k_{IM} + k_{D_1M} + k_{D_2M})[M^*] + k_{MD_1}[D_1^*] + k_{MD_2}[D_2^*]$$

$$\frac{d[D_1^*]}{dt} = k_{D_1M}[M^*] - (k_{FD_1} + k_{ID_1} + k_{MD_1} + k_{D_2D_1})[D_1^*] + k_{D_1D_2}[D_2^*]$$

$$\frac{d[D_2^*]}{dt} = k_{D_2M}[M^*] + k_{D_2D_1}[D_1^*] - (k_{FD_2} + k_{ID_2} + k_{MD_2} + k_{D_1D_2})[D_2^*] \quad \text{(A1)}$$

In the case of pulse excitation to produce $[M_o^*]$, i.e., the initially excited monomer molecules, I is supposed to be represented by a δ function. Then solving eq A1 with the initial condition that $[D_1^*] = [D_2^*] = 0$ at $t = 0$, we obtain eq A2. In eq A2a–c, A, B, and C are given by eq 17, and λ_1, λ_2, and λ_3 are the solutions of eq A3.

$$I_M(t) = k_{FM}[M_o^*]\{[k_{D_1D_2}(A-\lambda_2)(A-\lambda_3) - k_{D_1M}k_{MD_2}(C-\lambda_1) + k_{D_1D_2}k_{MD_1}k_{D_1M}][(\lambda_2-\lambda_1)(\lambda_1-\lambda_3)G]^{-1}[k_{MD_2}(B-\lambda_1) + k_{MD_1}k_{D_1D_2}]\exp(-\lambda_1 t) + [k_{D_1D_2}(A-\lambda_1) \times (A-\lambda_3) - k_{D_1M}k_{MD_2}(C-\lambda_2) + k_{D_1D_2}k_{MD_1}k_{D_1M}][(\lambda_3-\lambda_2) \times (\lambda_2-\lambda_1)G]^{-1}[k_{MD_2}(B-\lambda_2) + k_{MD_1}k_{D_1D_2}]\exp(-\lambda_2 t) + [k_{D_1D_2}(A-\lambda_1)(A-\lambda_2) - k_{D_1M}k_{MD_2}(C-\lambda_3) + k_{D_1D_2}k_{MD_1}k_{D_1M}][(\lambda_1-\lambda_3)(\lambda_3-\lambda_2)G]^{-1}[k_{MD_2}(B-\lambda_3) + k_{MD_1}k_{D_1D_2}]\exp(-\lambda_3 t)\} \quad \text{(A2a)}$$

$$I_{D_1}(t) = k_{FD_1}[M_o^*]\{[k_{D_1D_2}(A-\lambda_2)(A-\lambda_3) - k_{D_1M}k_{MD_2}(C-\lambda_1) + k_{D_1D_2}k_{MD_1}k_{D_1M}][(\lambda_2-\lambda_1)(\lambda_1-\lambda_3)G]^{-1}[k_{D_1D_2}(A-\lambda_1) + k_{D_1M}k_{MD2}]\exp(-\lambda_1 t) + [k_{D_1D_2}(A-\lambda_1) \times (A-\lambda_3) - k_{D_1M}k_{MD_2}(C-\lambda_2) + k_{D_1D_2}k_{MD_1}k_{D_1M}][(\lambda_3-\lambda_2) \times (\lambda_2-\lambda_1)G]^{-1}[k_{D_1D_2}(A-\lambda_2) + k_{D_1M}k_{MD_2}]\exp(-\lambda_2 t) + [k_{D_1D_2}(A-\lambda_1)(A-\lambda_2) - k_{D_1M}k_{MD_2}(C-\lambda_3) + k_{D_1D_2}k_{MD_1}k_{D_1M}][(\lambda_1-\lambda_3)(\lambda_3-\lambda_2)G]^{-1}[k_{D_1D_2}(A-\lambda_3) + k_{D_1M}k_{MD_2}]\exp(-\lambda_3 t)\} \quad \text{(A2b)}$$

$$I_{D_2}(t) = k_{FD_2}[M_o^*]\{[k_{D_1D_2}(A-\lambda_2)(A-\lambda_3) - k_{D_1M}k_{MD_2}(C-\lambda_1) + k_{D_1D_2}k_{MD_1}k_{D_1M}][(\lambda_2-\lambda_1)(\lambda_1-\lambda_3)G]^{-1}[(A-\lambda_1)(B-\lambda_1) - k_{MD_1}k_{D_1M}]\exp(-\lambda_1 t) + [k_{D_1D_2}(A-\lambda_1) \times (A-\lambda_3) - k_{D_1M}k_{MD_2}(C-\lambda_2) + k_{D_1D_2}k_{MD_1}k_{D_1M}][(\lambda_3-\lambda_2) \times (\lambda_2-\lambda_1)G]^{-1}[(A-\lambda_2)(B-\lambda_2) - k_{MD_1}k_{D_1M}]\exp(-\lambda_2 t) + [k_{D_1D_2}(A-\lambda_1)(A-\lambda_2) - k_{D_1M}k_{MD_2}(C-\lambda_3) + k_{D_1D_2}k_{MD_1}k_{D_1M}][(\lambda_1-\lambda_3)(\lambda_3-\lambda_2)G]^{-1} \times [(A-\lambda_3)(B-\lambda_3) - k_{MD_1}k_{D_1M}]\exp(-\lambda_3 t)\} \quad \text{(A2c)}$$

$$X^3 - (A+B+C)X^2 + (AB+BC+CA - k_{D_1M}k_{MD_1} - k_{D_2M}k_{MD_2} - k_{D_1D_2}k_{D_2D_1})X - (ABC - k_{D_2D_1}k_{MD_2}k_{D_1M} - k_{D_2M}k_{MD_1}k_{D_1D_2} - k_{D_2D_1}A - k_{D_2M}k_{MD_2}B - k_{D_1M}k_{MD_1}C) \quad \text{(A2d)}$$

B, and C are given by eq 17, and λ_1, λ_2, and λ_3 are the solutions of eq A3.

$$X^3 - (A+B+C)X^2 + (AB+BC+CA - k_{D_1M}k_{MD_1} - k_{D_2M}k_{MD_2} - k_{D_1D_2}k_{D_2D_1})X - (ABC - k_{D_2D_1}k_{MD_2}k_{D_1M} - k_{D_2M}k_{MD_1}k_{D_1D_2} - k_{D_2D_1}k_{D_1D_2}A - k_{D_2M}k_{MD_2}B - k_{D_1M}k_{MD_1}C) = 0 \quad \text{(A3)}$$

$$\lambda_3 > \lambda_2 > \lambda_1 > 0 \quad \text{(A4)}$$

$$G = k_{D_1D_2}k_{MD_2}(A-B) + k^2_{MD_2}k_{D_1M} - k_{MD_1}k^2_{D_1D_2} \quad \text{(A5)}$$

Here we will consider the two simplified models, that is, eq i and ii.

$$M^* \rightleftarrows D_2^* \rightleftarrows D_1^* \quad \text{(i)}$$

$$D_1^* \rightleftarrows M^* \rightleftarrows D_2^* \quad \text{(ii)}$$

In case i, k_{D_1M} is equal to zero. Therefore we can reduce eq A2b to eq A6. Similar equations are obtained for $I_M(t)$ and $I_{D_2}(t)$.

$$I_{D_1}(t) = \{[k_{FD_1}[M_o^*](A-\lambda_1)(A-\lambda_2)(A-\lambda_3)][(\lambda_3-\lambda_2) \times (\lambda_2-\lambda_1)(\lambda_1-\lambda_3)(A-B)]^{-1}\}[(\lambda_3-\lambda_2)\exp(-\lambda_1 t) - (\lambda_3-\lambda_1)\exp(-\lambda_2 t) + (\lambda_2-\lambda_1)\exp(-\lambda_3 t)] \quad \text{(A6)}$$

Here we can estimate whether each preexponential term has a positive or negative sign. A is the sum of the rate constants for the changes from excited monomers, and B is that from the normal excimer. According to Klöpffer[25] and Birks,[23,24] k_{FM} and k_{IM} are one order larger than k_{FD_1} and k_{ID_1}, respectively. Then it is quite reasonable to consider

$$A > B \quad \text{(A7)}$$

From the conditions that there should exist three different solutions in eq A3, we get eq A8. Thus under the conditions of the inequality A8, we obtain eq 8 from eq A2b.

$$\lambda_3 > A > \lambda_2 > B > \lambda_1 > 0 \quad \text{(A8)}$$

Next, let us consider another simplified case, case ii. $k_{D_1D_2} = k_{D_2D_1} = 0$ holds in this case. Therefore, we get eq A7 as each fluorescence response function.

$$I_M(t) = \{(k_{FM}[M_o^*])/[(\lambda_3-\lambda_2)(\lambda_2-\lambda_1)(\lambda_1-\lambda_3)]\}[(\lambda_3-\lambda_2)(\lambda_1-C)(B-\lambda_1)\exp(-\lambda_1 t) + (\lambda_1-\lambda_3)(\lambda_2-C)(B-\lambda_2)\exp(-\lambda_2 t) + (\lambda_2-\lambda_1)(\lambda_3-C)(B-\lambda_3)\exp(-\lambda_3 t)] \quad \text{(A9a)}$$

$$I_{D_1}(t) = \{(k_{FD_1}k_{D_1M}[M_o^*])/[(\lambda_3-\lambda_2)(\lambda_2-\lambda_1) \times (\lambda_1-\lambda_3)]\}[(\lambda_3-\lambda_2)(\lambda_1-C)\exp(-\lambda_1 t) + (\lambda_1-\lambda_3)(\lambda_2-C)\exp(-\lambda_2 t) + (\lambda_2-\lambda_1)(\lambda_3-C)\exp(-\lambda_3 t)] \quad \text{(A9b)}$$

$$I_{D_2}(t) = \{(k_{FD_2}[M_o^*])/[k_{MD_2}(\lambda_3-\lambda_2)(\lambda_2-\lambda_1)(\lambda_1-\lambda_3)]\}\{(\lambda_3-\lambda_2) \times (C-\lambda_1)[k_{D_1M}k_{MD_1} - (A-\lambda_1)(B-\lambda_1)]\exp(-\lambda_1 t + (\lambda_1-\lambda_3)(C-\lambda_2)[k_{D_1M}k_{MD_1} - (A-\lambda_2)(B-\lambda k_2)]\exp(-\lambda_2 t) + (\lambda_2-\lambda_1)(C-\lambda_3)[k_{D_1M}k_{MD_1} - (A-\lambda_3)(B-\lambda_3)]\exp(-\lambda_3 t)\} \quad \text{(A9-c)}$$

From the conditions that there exist three different solutions in eq A3, we get the alternative inequalities

$$\lambda_3 > B > \lambda_2 > C > \lambda_1 > 0 \quad \text{(A10)}$$

$$\lambda_3 > C > \lambda_2 > B > \lambda_1 > 0 \quad \text{(A11)}$$

Then we obtain eq 11 in the case of inequality A10, while we obtain eq 12 in the case of inequality A11.

Registry No. I, 15971-29-6; II, 7770-45-8; III, 24764-66-7; IV, 34225-15-5; BMNP, 34225-14-4; BHNP, 77012-76-1.